Mechanisms of optical gain in heavily doped $Al_xGa_{1-x}N$:Si structures ($x = 0.56-1$)

© P.A. Bokhan[1], K.S. Zhuravlev[1], D.E. Zakrevsky[1,2], T.V. Malin[1], N.V. Fateev[1,3,¶]

[1] Rzhanov Institute of Semiconductor Physics Siberian Branch of Russian Academy of Sciences,
630090 Novosibirsk, Russia
[2] Novosibirsk State Technical University,
630073 Novosibirsk, Russia
[3] Novosibirsk State University,
630090 Novosibirsk, Russia
¶ E-mail: fateev@isp.nsc.ru

Received October 3, 2023
Revised November 10, 2023
Accepted November 11, 2023

The optical gain parameters in the six heavily doped $Al_xGa_{1-x}N$:Si structures with $x = 0.56$, 0.62, 0.65, 0.68, 0.74, were experimentally studied at room temperature. Under optical excitation by pulsed radiation with $\lambda = 266$ nm, the mechanisms of stimulated emission of radiative recombination of nonequilibrium charge carriers, leading to the appearance of broadband radiation in the wide range (350–650 nm) of the spectrum with a high luminescence quantum yield are studied. High optical gain ($> 10^3$ cm^{-1}) are realized due to the good optical quality of the structures, large donor-acceptor recombination cross sections ($\sim 10^{-15}$ cm^2) and the high density (up to 10^{20} cm^{-3}) of radiative recombination centers.

Keywords: heavily doped $Al_xGa_{1-x}N$ structures, optical gain, electron-acceptor recombination, donor-acceptor recombination, AlN/GaN heterostructure, two-dimensional hole gas, *p*-channel transistor, polarization.

DOI: 10.61011/SC.2023.09.57433.5627

1. Introduction

The creation of new, powerful, efficient and compact semiconductor radiation sources of both coherent and incoherent nature of various spectral ranges is an urgent task. This applies to devices that generate broadband radiation of the visible range and narrow lines of laser radiation with the possibility of continuous tuning of the generation frequency in a significant spectral range. Such devices have numerous possible applications in biology, medicine, optical communications, information display and display devices, etc., as energy-saving, durable and environmentally friendly radiation sources with a continuous spectrum and laser sources with high light and energy efficiency [1–3]. It is from this point of view that group III metal nitrides and their solid solutions, which are straight-band semiconductors with a band gap covering a wide range from 0.7 eV for InN to 6.2 eV for AlN, are interesting and promising as active media, which corresponds to a wavelength range of 200–1770 nm. It should be noted that much-needed efficient sources of green light $\lambda = 530-560$ nm, which corresponds to the maximum sensitivity of human eyes have not been created yet. The use of optical transitions through defect levels in a wide-band (with an adjustable band gap in the range of 3.4–6.2 eV) in a solid solution of AlGaN, heavily doped with silicon is promising for the implementation of green LEDs and laser diodes [4,5]. The wide spectrum of defect radiation in AlGaN provides the basis for the creation of light sources ranging from blue-green to the near IR band of the spectrum (almost the entire visible range) and lasers with unique parameters — with tunable wavelength in a broad range of wavelengths and frequencies (up to 500 THz).

The purpose of this work is to study the physical mechanisms of optical gain in heavily doped $Al_xGa_{1-x}N$:Si structures in case of an optical pumping. The processes of excitation, recombination and optical gain were studied (and the results of previous experimental studies were also analyzed) for $Al_xGa_{1-x}N$:Si-structures with a molar fraction $x = 0.56$, 0.62, 0.65, 0.68, 0.74, 1 and their general patterns were determined for the optical properties and mechanisms of optical gain.

2. Methods and experimental results

The studied $Al_xGa_{1-x}N$:Si-structures with a molar fraction of aluminum $x = 0.56$, 0.62, 0.65, 0.68, 0.74, 1 they were grown by molecular beam epitaxy. Films with a thickness of $l = 1.2\,\mu$m on substrates of nitrided sapphire with an orientation of (0001) and a thickness of 0.43 mm were grown at a temperature of 860°C in an ammonia flow of 130 cm^3/min at the total pressure of the mixture of $5 \cdot 10^{-5}$ Torr. Buffer AlN films with a thickness of 350 nm were grown in advance on a sapphire substrate. The aluminum content x in the AlGaN layers was determined by the ratio of Al/Ga fluxes during the growth process. The doping was performed by a silane flux SiH_4 (0.7%) diluted in nitrogen N_2, with the

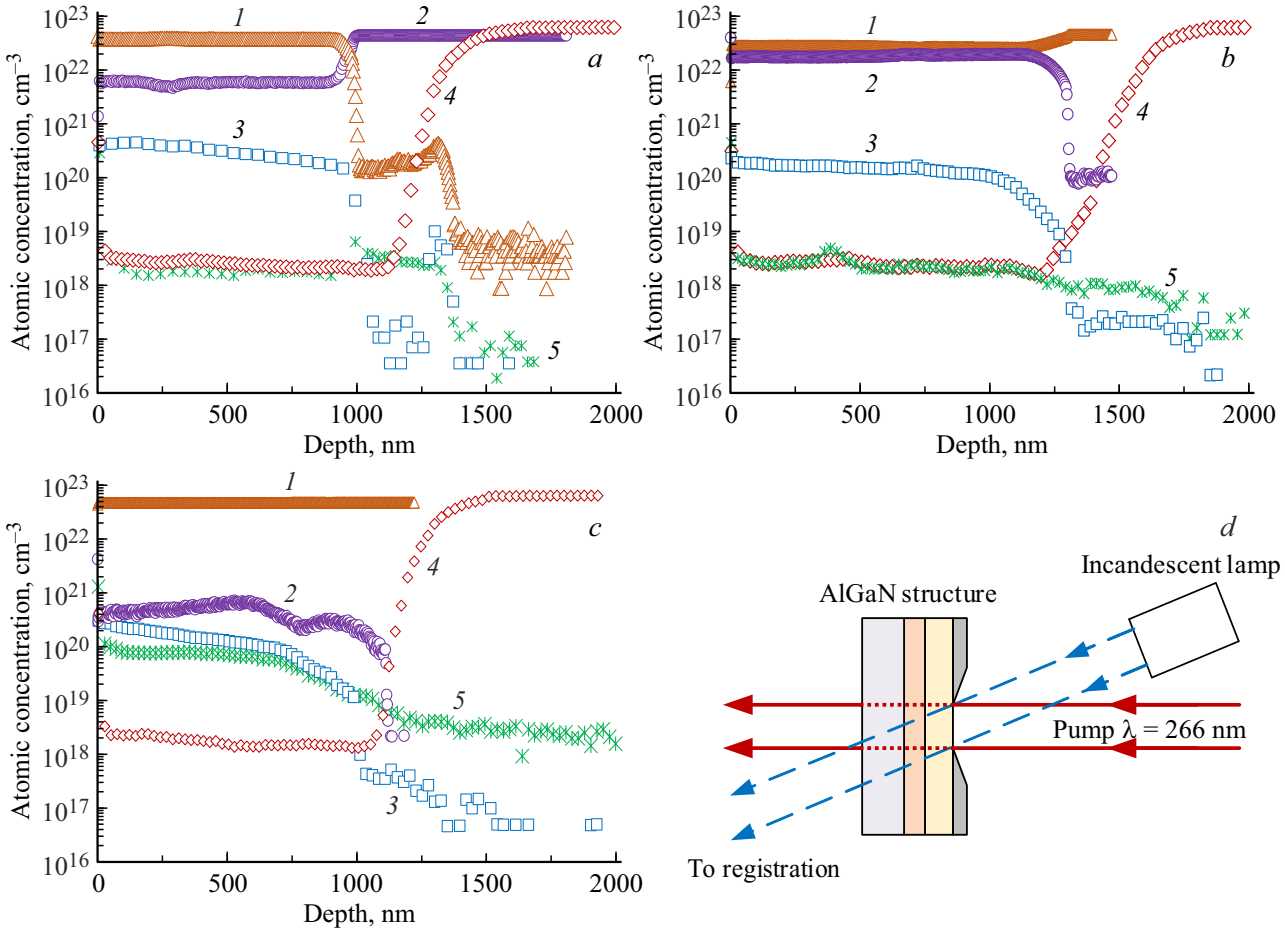

Figure 1. SIMS analysis for $Al_xGa_{1-x}N$:Si-structures: *a* — $x = 0.56$, *b* — $x = 0.62$, *c* — $x = 1$, (*1* — Al, *2* — Ga, *3* — Si, *4* — O, *5* — C); *d* — experimental scheme for measuring optical gain. (Colored version of the figure is presented in electronic version of the article).

doping level n_{Si} exceeding 10^{20} cm^{-3}. The synthesis process and measurement of the parameters of AlGaN films are described in [6]. The results of secondary ion mass spectrometry (SIMS) were used to characterize the structures using primary ions C_s^+ with neutralization of the charging of samples by their irradiation with an electron beam and use of high mass resolution. The concentrations of silicon, aluminum, gallium, oxygen and carbon atoms for $Al_xGa_{1-x}N$:Si-structures with $x = 0.65$, 0.68, 0.74 are given in [5–7], and for structures with $x = 0.56$, 0.62 and 1 these concentrations are provided in Figure 1, *a*–*c*. Studies of the morphology of the surface of the structure with an atomic force microscope showed that all the studied samples have a smooth surface with RMS roughness of < 5 nm.

The method of direct measurement of the intensity gain of a test wave propagating at an angle 15° to the normal of the structure is used to determine the values of the optical gain coefficients [8]. The experiment setup is shown in Figure 1, *d*. An incandescent lamp with a continuous radiation spectrum, which was formed by light filters in the desired spectral range, was used as a source of test radiation. Optical pumping of the structures was carried out by radiation of the fourth harmonic of Nd:YAG laser with $\lambda_p = 266$ nm, with a pumping pulse half-maximum time of $\tau_p = 8$ ns and with a pulse repetition rate of 10 Hz. The pumping radiation illuminated the diaphragmatic area with a diameter of 3 mm of the film $Al_xGa_{1-x}N$:Si to the normal of the surface of the structure. The test radiation, together with luminescence radiation and stimulated radiation of the structure, was focused into the core of a quartz fiber with a diameter of 1 mm. Spectrometer Kolibri 2 [9] with a resolution of 0.5 nm was used for registration of the radiation spectrum at the output of the waveguide. In another case, the radiation was transmitted to a monochromator SPM-2, which functioned as a spectral filter with a half maximum bandwidth of 7–14 nm (depending on the wavelength) and was recorded by a photoelectronic multiplier with a time resolution of 5 ns, the signal from which was measured by Tektronix oscilloscope (TDS2024B). The pumping radiation power was measured by a thermal power sensor head (Thorlabs, S401C). All experiments were performed at room temperature.

To determine the gain at a fixed wavelength we measured (see Figure 1, *d*) the time behavior of the intensity of

luminescence $I_{LP}(t)$ recorded in the presence of continuous test radiation from an incandescent lamp with an intensity of I_{pi} and $I_{L0}(t)$ — luminescence intensity without test radiation. The difference in the amplitudes of these curves, normalized to a constant amplitude of the test radiation I_{pi}, expresses the time dependence of the gain in the studied structure

$$G(tk) = \big(I_{LP}(tk) - I_{L0}(tk)\big)/I_{pi}.$$

The absolute values of the optical gain G for each structure at fixed values of pumping power and radiation wavelength were determined by the formula

$$G = (t_m)^{-1} \sum_{k=0}^{k=m} G(t_k)\Delta t, \qquad (1)$$

where the time interval between the measured points is set from 0 to t_m, and $\Delta t = (1-5)$ ns. The maximum measurement time was $t_m = (10-50)\,\mu$ s and was selected from the condition when the time-decreasing value $G(t_m)$ becomes comparable to noise. The optical gain of the test radiation g_0 passing through the excited structure a distance of length (thickness $Al_xGa_{1-x}N$:Si of the film) $l = 1.2\,\mu$m, was determined using the following formula

$$g_0 = [\ln(G)]/l. \qquad (2)$$

Figure 2 shows typical experimental dependences of the time behavior of luminescence intensity $I_{L0}(t)$ and gain $G(t)$ for $Al_{0.62}Ga_{0.38}N$ structures with pumping power density of $P_p = 530\,\text{kW/cm}^2$. The behavior of these curves demonstrates the presence of two components of radiative recombination [5]: the first — is a fast component, with an exponential decline in several tens of nanoseconds, and the second — slow component, with a hyperbolic attenuation law and a characteristic time — tens of microseconds. The dashed line in Figure 2 shows the boundary located at the inflection point of the attenuation curves separating the fast and slow components.

The fast component associated with the process of $e-A$ recombination with photon emission is described by the exponent [6]

$$I_f(t) = A_1 \exp(t/\tau_f), \qquad (3)$$

where A_1 is a constant, and τ_f is the luminescence decay time for $e-A$ recombination.

The slow component associated with the recombination of donor-acceptor pairs — the DA recombination process is described by the hyperbolic function [6,10]

$$I_s(t) = B_1/(t + \tau_s), \qquad (4)$$

where B_1 — constant, τ_s — luminescence decay time for DA recombination. The total luminescence intensity is the sum of:

$$I_0(t) = I_f(t) + I_s(t). \qquad (5)$$

Interpolation of equation (5) according to experimental data by the least squares method gives numerical values

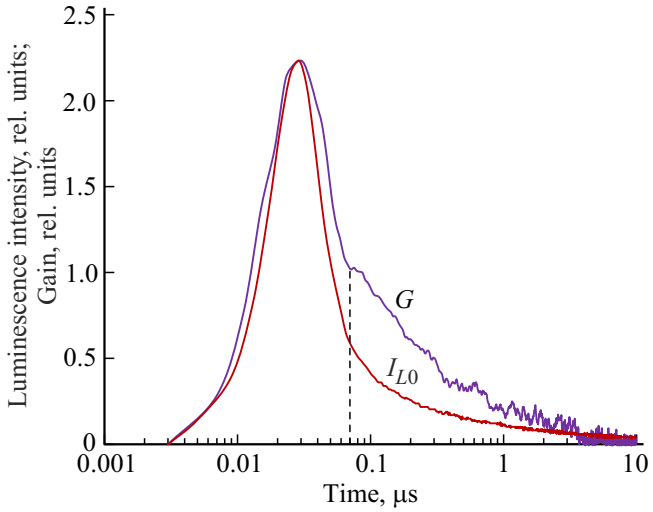

Figure 2. Time dependences of attenuation of luminescence intensities $I_{L0}(t)$ and optical gain of $G(t)$ at $P_p = 530\,\text{kW/cm}^2$. Vertical dashed line — the boundary separating the fast and slow components.

of the parameters in the equations (1), (2), describing the coefficients A_1, B_1 and the times τ_f, τ_s.

The parameters characterizing the studied structures, as well as the results of experimental studies and calculations are listed in the table.

Since the fractions of the absorbed pumping power for each structure are different (see the table), in subsequent comparative studies of optical amplification for all studied structures, the pumping power densities P_p were selected in such a way that the density of photons absorbed in one pumping pulse was the same and amounted to a value determined by according to the formula

$$N_{ph}(\text{cm}^{-3}) = 0.89 \cdot 10^{14} \alpha P_p(\text{W/cm}^2)$$
$$\approx 9 \cdot 10^{19}\,\text{phot/cm}^3, \qquad (6)$$

where α — the fraction of absorbed pumping energy that passed through the structure perpendicular to its surface (see table). Due to the high quantum yield of luminescence, the value of N_{ph} approximately coincides with the concentration of nonequilibrium electrons formed after the action of pumping laser radiation and determining radiative recombination.

Figure 3 shows the full luminescence spectra (dotted curves) at one value $N_{ph} \approx 9 \cdot 10^{19}\,\text{phot/cm}^3$. Here, too, solid lines represent the luminescence spectra that have passed through a monochromator with an output slit width of 1 mm. A shift of the maxima of the total radiation spectra to the shortwave region by the value of ~ 0.02 eV is observed in all studied structures with a 10 fold increase in the pumping intensity. This experimental fact further confirms that the observed radiation is associated precisely with the process of donor-acceptor recombination.

Parameters of $Al_xGa_{1-x}N$:Si-structures and experimental results

x	E_g, eV	η	λ_0, nm	α, %	ε	n_0	σ_0, 10^{-16} cm^2	R^2, 10^{-16} cm^2	$\Delta\lambda$, nm	τ_f, ns	σ_f 10^{-16} cm^2	g_f/g_0
0.56	4.67	0.37	546.3	95	8.94	2.2	17	10.4	13.5	14	1.2	1.1
0.62	4.89	0.47	533.2	58.8	8.88	2.19	11	9.6	12.7	15	1.1	1.2
0.65	4.94	0.49	507.6	49.6	8.85	2.19	9.8	9.6	11.8	14	1	2
0.68	5.03	0.57	486.3	24.8	8.82	2.18	9.5	11.1	10.7	18	1.1	5
0.74	5.22	0.79	473.6	18.8	8.76	2.17	6.5	11.1	9.7	22	0.9	1.5
1	6.13	0.47	441.3	8.7	8.5	2.12	3.3	5.8	7.3	15	1	3.4

Note. x — molar fraction of Al in $Al_xGa_{1-x}N$-structure; E_g — the width of the band gap [15]; η — quantum yield of structures [7] (for $x = 0.62$ value η obtained from interpolation of experimental data); α — the proportion of absorbed pumping energy; λ_0 — the wavelength of the center luminescence spectrum; ε — dielectric constant of structures [17]; n_0 — refraction index $Al_xGa_{1-x}N$:Si-films [15]; σ_0 — experimental value of the cross section for complete recombination; R^2 — calculated values of the stimulated emission cross section for *DA* recombination; $\Delta\lambda$ — the width of the luminescence emission spectrum transmitted through the monochromator; τ_f — the decay time of the fast component of stimulated emission; σ_f — calculated values of the stimulated emission cross section for rapid recombination. g_f/g_0 ratio at the density of absorbed photons $N_{ph} \geq 2 \cdot 10^{19}$ cm^{-3}.

Figure 4 shows the measured experimental dependences of the optical gain coefficient g_0 on the photon density N_{ph}. The gain g_0 exceeds 10^3 cm^{-1} with the density of absorbed photons of $N_{ph} > 10^{19}$ cm^{-3}. The general values of the cross section of the stimulated emission process σ_0 for each of the structures were determined based on these dependencies, using linear sections of curves according to the formula [11]

$$\sigma_0 = g_0/(\eta \cdot N_{ph}), \qquad (7)$$

where η determines the quantum luminescence yield of structures [7] (see table). The quantum yield values for a structure with $x = 0.62$ were calculated using the results of interpolation of the quantum yield values by a linear function in the range of $x = 0.47-0.74$. The obtained values σ_0 are provided in the following table. The nature of gain saturation, which is observed in structures with small values $x = 0.56$, 0.62 and 0.65, has not been studied in this work.

Figure 5 shows the experimental dependences of g_f/g_0 — the ratio of the fast components of the optical gain

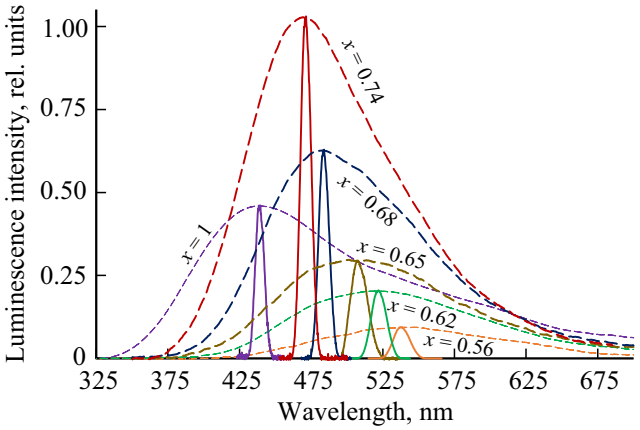

Figure 3. Luminescence spectra of the studied $Al_xGa_{1-x}N$:Si-structures. Narrow peaks represent luminescence spectra at the maximum of a wide spectrum transmitted through a luminescence monochromator, with an output slit width of 1 mm.

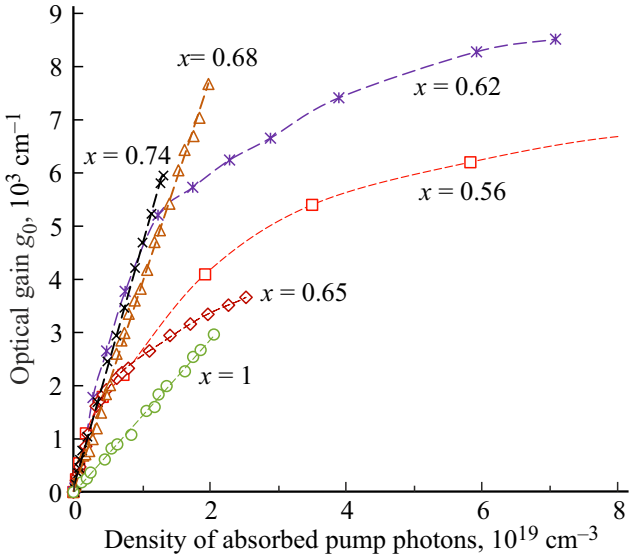

Figure 4. Dependences of optical gain coefficients g_0 depending on the density of absorbed pump photons N_{ph}.

coefficients g_f to the total value of the gain coefficient g_0 for the studied structures on the density of absorbed pumping photons. The ratio g_f/g_0 does not exceed 20% in the region of small values of pumping energy and decreases to several percent with increasing pumping power. These results confirm that the process associated with the recombination of donor-acceptor pairs is dominant.

3. Results and discussion

When considering the gain mechanisms in structures, it becomes necessary to consider the nature of recombination processes at all stages after absorption of pumping radiation in structures. The donor and acceptor levels consist of wide bands in the band gap due to the heavy silicon doping $n_{Si} > 10^{20}$ cm^{-3}. In the equilibrium state, electrons from

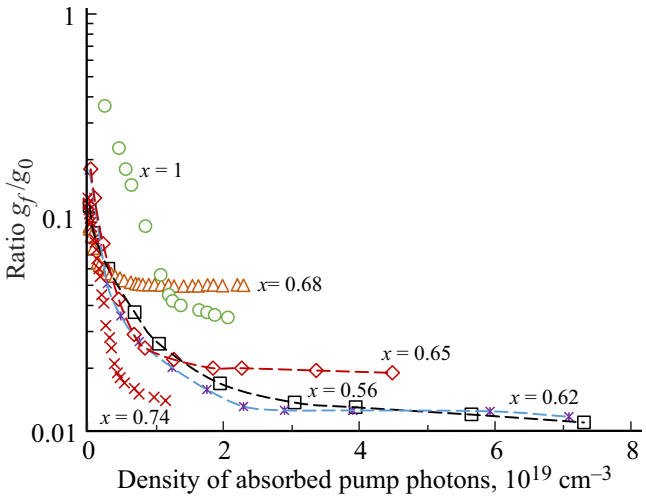

Figure 5. Relationship dependencies g_f/g_0 fast optical gain component g_f to the total gain value g_0 depending on the density of absorbed pumping photons N_{ph}.

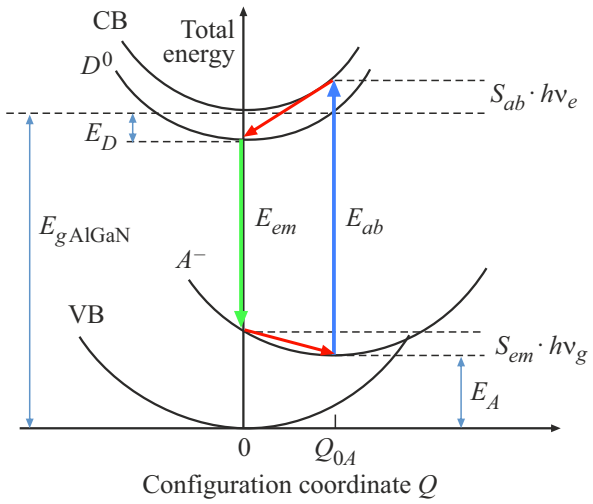

Figure 6. A configuration diagram describing optical transitions. The blue and green arrows indicate optical transitions during excitation and recombination, respectively. The red arrows indicate non-radiative recombination, bringing the system to an equilibrium state. (The colored version of the figure is available on-line).

donors D move to acceptors A, thus, there are D^+-, D^0- and A^--centers in the volume of the structure.

At the first stage, pulse pumping energy is absorbed, as a result of which electrons are detached from negatively charged acceptors, which pass into the conduction band, and negatively charged acceptors become neutral. At the second stage, nonradiative relaxation occurs which results in the transition of electrons in the conduction band into an excited stationary state with lower energy in a short time $\sim 10^{-12}$ s. This is illustrated by the configuration diagram in Figure 6, representing possible optical transitions. The third stage is characterized by the transition of the system to an equilibrium state due to the process of radiative recombination. There are two main competing processes causing it. First, nonequilibrium electrons can be captured by positively charged donors. After which, neutral donors radiatively interact with neutral acceptors for the system to come to equilibrium. As a result, photons are produced due to the slow (luminescence decay time $> 10\,\mu$s) recombination process DA, which form a wide band with energy

$$E_{DA} = E_g - E_D - E_A + E_q, \tag{8}$$

where E_g — band gap, E_D and E_A —ionization energies of donors and acceptors, E_q — Coulomb energy. Secondly, nonequilibrium electrons can be captured by neutral acceptors with rapid (luminescence decay time > 10 ns) photon emission due to $e-A$ recombination with energy:

$$E_{eA} = E_g - E_A. \tag{9}$$

Broad radiation spectra shown in Figure 3 are formed as a result of these two processes. The last term in equation (8) can be calculated from equation [12,13]

$$E_q = e^2/\varepsilon R_m = \Delta E_{1/2}/0.76, \tag{10}$$

where R_m — the distance between the donor and the acceptor at the maximum of the spectrum, $\Delta E_{1/2}\,(\text{eV}) = 1.24 \cdot \left(1/\lambda_2\,(\mu\text{m}) - 1/\lambda_1\,(\mu\text{m})\right)$ — the width of the spectra at half the height of the luminescence spectra. From here, it is possible to determine the values R_m, at which the maximum intensity value in the radiation spectra for each structure is realized. From these values, the value of the cross section of the radiative DA recombination is calculated, which is approximately defined as R_m^2 [12,13]. The obtained calculation results presented in the table satisfactorily coincide with the experiment, which confirms the validity of the model under consideration. It should be noted that the obtained values of the cross sections σ_0 are an order of magnitude higher than the values for the GaAs laser [11].

The process cross section for $e-A$ recombination can be calculated using the formula for a nonuniformly broadened radiation spectrum [14]:

$$\sigma_f = 0.47(\lambda_0^4/\Delta\lambda)/4\pi c\tau n_0, \tag{11}$$

where λ_0 — the peak wavelength of the radiation, $\Delta\lambda$ — the full width at half the height of the spectra recorded at the output of the monochromator, τ — the decay time of the stimulated emission intensity measured at the maximum spectrum, c — speed of light, n_0 — refractive index of $Al_xGa_{1-x}N$-films [15]. The spectra and time of decay of the intensity of stimulated emission radiation transmitted through a monochromator at a wavelength at the maximum of the radiation spectrum λ_0 were used to determine the parameters necessary for calculation according to the formula (10). The obtained values of the radiative recombination cross sections σ_f are shown in the

table and are almost an order of magnitude smaller than the cross sections for *DA* recombination.

Figure 5 and the table shows the values of the ratio of the gain for the processes of $e-A$ recombination g_f and the total gain g_0 of the density of absorbed photons. Using equation (6), it is possible to obtain the ratio of concentrations of acceptors N_A and donors N_D responsible for radiative $e-A$ and *DA* recombination according to the formula

$$(N_A/N_D) \sim (g_f/g_0)/(\sigma_f/\sigma_0). \quad (12)$$

Calculations show that the ratio N_A/N_D for various structures takes values in the range $0.1-0.5$. The obtained values N_A/N_D significantly exceed the calculation results from the known values of the capture cross sections of nonequilibrium electrons on positively charged donors and neutral acceptors.

Electrons and charged recombination centers, which are positively charged donors, interact due to electrostatic forces of attraction. An electron is trapped if it approaches the center at a distance of r, at which the electrostatic energy of its interaction with the center is greater than or equal to the average kinetic energy of thermal motion. In this case, it is possible to estimate the capture cross section $\sigma_D \sim \pi r^2 \sim 10^{-12}\,\mathrm{cm}^2$ at $\varepsilon \approx 8.5$ and $T = 300\,\mathrm{K}$. Then the rate of electron capture by a positively charged donor is $\mathrm{W}_D \sim (\sigma_D \cdot N_D \cdot \nu_e) \sim 10^{15}\,\mathrm{s}^{-1}$, where $N_D \sim 10^{20}\,\mathrm{cm}^{-3}$, $\nu_e \sim 10^7\,\mathrm{cm/s}$ — the velocity of the electron. For neutral electron recombination centers, which are neutral acceptors, the capture cross section should have the order of the geometric size of the atom, i.e. $\sigma_A \sim 10^{-15}\,\mathrm{cm}^2$. In this case, the rate of electron capture by neutral acceptors is $W_A \sim (\sigma_A \cdot N_A \cdot \nu_e) \sim 10^{11}\,\mathrm{s}^{-1}$, where $N_A \sim 10^{19}\,\mathrm{cm}^{-3}$, which is 4 orders of magnitude less than W_D. Consequently, the concentrations of captured centers by donors are 4 orders of magnitude higher than on acceptors, i.e. $N_A/N_D \sim 10^{-4}$. The obtained values are 3 orders of magnitude less than the experimentally observed ones. The most likely reason for this difference is related to the process of rapid electron capture by a neutral acceptor with time $\tau_A \sim 1/W_A \sim 10^{-11}\,\mathrm{s}$. As result, the $\sim 8 \cdot 10^3$ acts of ionization and electron capture on acceptors take place during the pumping pulse since the duration of the laser pulse of pumping radiation $\tau_p = 8\,\mathrm{ns}$ is significantly longer than τ_A. These processes significantly increase the pulse duration and radiation intensity of $e-A$ recombination.

The time of electron capture by a positively charged donor in case of slow *DA* recombination is $\tau_D \sim 1/W_D \sim 10^{-15}\,\mathrm{s}$, i.e., is even less. However, due to the small overlap of the wave functions, carriers have longer lifetimes significantly exceeding the duration of pumping pulses for donor-acceptor pairs [12]. As a result, only one act of electron capture by the donor takes place during the action of the pumping pulse. The values for *DA* recombination section in the structure with $x = 1$ in ~ 2 times smaller compared to other structures. More studies are needed to find it out.

4. Conclusion

Optical gain coefficients were measured for six $Al_xGa_{1-x}N$:Si structures with $x = 0.56$, 0.62, 0.65, 0.68, 0.74, 1 with optical pumping as a result of the experiments. The main process of generation of broadband radiation in the visible range of the spectrum is donor-acceptor recombination with a stimulated emission cross section $\sim 10^{-15}\,\mathrm{cm}^2$ and a maximum concentration of recombination centers $\sim 10^{20}\,\mathrm{cm}^{-3}$.

The configuration diagram (Figure 6), representing the optical transitions [6], reproduces quite accurately the four-level scheme of stimulated emission generation in lasers. The recombination mechanisms of nonequilibrium charge carriers according to this scheme have a number of advantages, since in this case small pumping powers are required to achieve threshold gain, which is observed experimentally ($\sim 6.5\,\mathrm{kW/cm}^2$ for stimulated emission in $Al_{0.68}Ga_{0.38}N$-structure [16]).

Funding

This study was carried out under state assignment FWGW−2022−0012.

Conflict of interest

The authors declare that they have no conflict of interest.

References

[1] X. Zhao, K. Sun, S. Cui, B. Tang, H. Hu, S. Zhou. Adv. Photon. Res., **4**, 2300061 (2023).
[2] J. Wierer, N. Tansu. Laser Photon. Rev., **13**, 1900141 (2019).
[3] J.Y. Tsao, S. Chowdhury, M.A. Hollis, D. Jena, N.M. Johnson, K.A. Jones, R.J. Kaplar, S. Rajan, C.G. Van de Walle, E. Bellotti, C.L. Chua, R. Collazo, M.E. Coltrin, J.A. Cooper, K.R. Evans, S. Graham, T.A. Grotjohn, E.R. Heller, M. Higashiwaki, M.S. Islam, P.W. Juodawlkis, M.A. Khan, A.D. Koehler, J.H. each, U.K. Mishra, R.J. Nemanich, R.C.N. Pilawa–Podgurski, J.B. Shealy, Z. Sitar, M.J. Tadjer, A.F. Witulski, M. Wraback, J.A. Simmons. Adv. Electron. Mater., **4**, 1600501 (2018).
[4] P.A. Bokhan, N.V. Fateev, T.V. Malin, I.V. Osinnykh, D.E. Zakrevsky, K.S. Zhuravlev. Optical Mater., **105**, 109879 (2020).
[5] P.A. Bokhan, N.V. Fateev, T.V. Malin, I.V. Osinnykh, D.E. Zakrevsky, K.S. Zhuravlev. J. Luminesc., **252**, 119392 (2022).
[6] I.V. Osinnykh, T.V. Malin, D.S. Milakhin, V.F. Plyusnin, K.S. Zhuravlev. Jpn. J. Appl. Phys., **58**, SCCB27 (2019).
[7] P.A. Bokhan, N.V. Fateev, T.V. Malin, I.V. Osinnykh, Dm.E. Zakrevsky, K.S. Zhuravlev. J. Luminesc., **203**, 127 (2018).
[8] P.A. Bokhan, K.S. Zhuravlev, Dm.E. Zakrevsky, T.V. Malin, I.V. Osinnykh, N.V. Fateev. Pisma ZhTF, **45** (18), 48 (2019). (in Russian).
[9] I.A. Zarubin, V.A. Labusov, S.A. Babin. Zavod. lab. Diagnostika materialov, **85**, *1*, 117, (2019). (in Russian).
[10] B. Guo, Z.R. Qiu, K.S. Wong. Appl. Phys. Lett., **82**, 2290 (2003).

[11] O. Zvelto. *Principy lazerov* (M., Mir, 1990) p. 560. (in Russian).
[12] D.G. Thomas, J.J. Hopfield, W.A Augustyniak. Phys. Rev., **140**, A202 (1965).
[13] VF. Agekyan, N.R. Grigoryeva. *Lyuminescenciya poluprovodnikovykh kristallov* (SPb., Izd-vo Sankt-Peterburgskogo gos. un-ta, 2016) p. 155. (in Russian).
[14] S. Kück. Appl. Phys. B, **72** 515 (2001).
[15] U. Özgur, G. Webb.Wood, H.O. Everitt, F. Yun, H. Morkoç. Appl. Phys. Lett., **79**, 4103 (2001).
[16] P.A. Bokhan, K.S. Zhuravlev, Dm.E. Zakrevsky, T.V. Malin, I.V. Osinnykh, N.V. Fateev. FTP, **56** (12), 1125 (2022). (in Russian).
[17] R. Quay. *Gallium Nitride Electronics* (Springer–Verlag, Berlin–Heidelberg, 2008) p. 470.

Translated by Ego Translating